ISBN: 978-3-95450-184-7 doi:10.18429/JACoW-IPAC2018-WEPAL058

# BEAM LOSS STUDIES AT THE TAIWAN PHOTON SOURCE

C. H. Huang†, Demi Lee, Jenny Chen,Y. S. Cheng, K. H. Hu, C. Y. Wu, K. T. Hsu,
NSRRC, Hsinchu 30076, Taiwan

*Abstract*

PIN-photodiodes and RadFETs are installed in the storage ring of the Taiwan Photon Source (TPS) to study beam loss distributions and mechanisms. In the highest dose area, the radiation comes mainly from hard X-rays produced by synchrotron bending magnets. During beam cleaning and after replacing a vacuum chamber, losses due to inelastic Coulomb scattering occur mostly downstream from bending magnets while elastic scattering causes electrons to get lost mainly after an elliptically polarizing undulator which has a limited vertical aperture. During the injection period, the beam loss pattern can be changed by modifying injection conditions or lattice settings. The beam loss usually happens in the injection section and small-aperture section. The injection efficiency can be improved by minimizing the detected injection loss.

## INTRODUCTION

The Taiwan Photon Source (TPS) is a third-generation light source at the NSRRC [1] with a storage ring circumference of 518.4 m and 24 double-bend achromatic cells. To study beam loss during operation, radiation-sensing field-effect transistors (RadFETs) [2] and Bergoz's PIN-diode beam loss monitors (BLMs) are installed in the storage ring [3]. The RadFET, a discrete p-channel metal-oxide-semiconductor field-effect transistor optimized for ionizing radiation, is used to measure the accumulated dose [4] whereas the PIN-diode BLM is designed to detect and count charged particles during a pre-set time interval [5].

At first, radiation patterns at the TPS and their sources for high radiation areas are studied. Beam loss mechanisms and patterns during poor vacuum pressure condition are discussed. Finally, beam loss locations during injection are summarized to provide guidance information for improvement of the injection efficiency.

## EXPERIMENTAL SETUP

Six RadFETs and six PIN-diode BLMs are attached to the vacuum chamber on the inside towards the ring centre of each cell as shown in Fig. 1. The threshold voltage of the RadFET, corresponding to the accumulated dose with a pre-recorded calibration curve, is read by a home-made reader [4]. The dose rate is calculated with the EPICS record processing system and data acquisition for the PIN-diode BLMs is performed by a scaler. All scalers are synchronized by the timing system of the accelerator [5]. The accumulated dose of the RadFETs and counting rates of the PIN-diode BLMs are both shown in the control system for on-line reading. The threshold voltages of the RadFETs and counting rates of the Pin-diode BLMs are stored in the archive system for further analysis.

† huang.james@nsrrc.org.tw

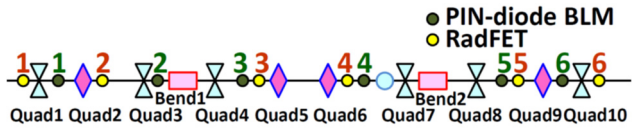


Figure 1: The installation position of six RadFETs and PIN-diode BLMs in each cell. The RadFETs and PIN-diode BLMs in each cell are labelled as position 1 to 6.

## BEAM LOSS DISTRIBUTION STUDY

During top-up injection from 300 mA to 302 mA or during decay mode, the highest detected dose rates are mainly located at positions #4 and #6 for the RadFETs in Fig. 2(a) and (b). During injection at low current, the detected dose rate is much lower and the detected dose rate is roughly proportional to the beam current. For the PIN-diode BLMs, the highest counting rate is mainly at position #4 rather than position #6 in Fig. 2(c) and (d). The locations of the RadFET and PIN-diode at position #4 are close but at position #6 they are different with one after and one before the 10th quadrupole.

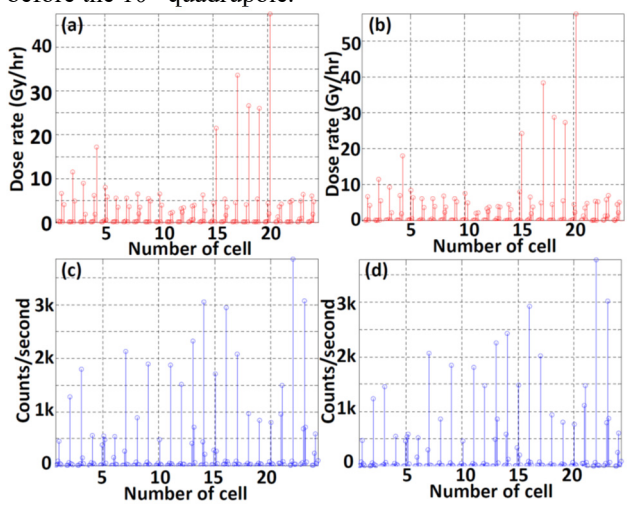


Figure 2: Radiation distribution detected by RadFETs and PIN-diode BLMs in top-up mode (a,c) and decay mode (b,d), respectively.

In order to determine the location with the largest radiation dose rate, a RadFET setup for higher intensities has been implemented after the 1st and 2nd bending magnet. Results show that the high dose rate occurs between the 6th and 7th quadrupoles and after the 10th quadruple. This explains why the counting rates of the PIN-diode at position #6 are low.

## RADIATION SOURCE AT HIGH DOSE RATE REGION

In the high dose rate region, a degradation of magnet epoxy and cable ties has been found. The colour of the magnet epoxy and cable ties turned yellow from white, as

ISBN: 978-3-95450-184-7 doi:10.18429/JACoW-IPAC2018-WEPAL058

shown in Fig. 3. The colour of the cable tie is darker on the outside-wall of the vacuum chamber (+X) compared to the inside-wall (-X).

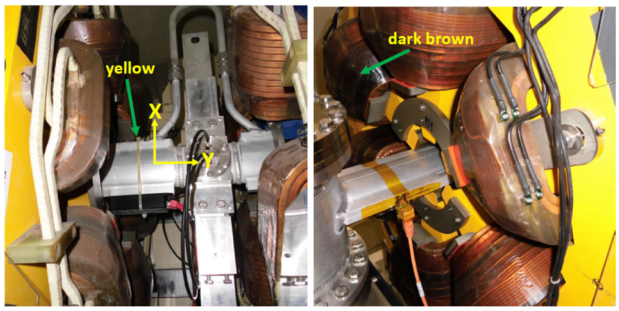


Figure 3: Degradation of magnet epoxy and cable tie due to radiation.

When the RadFETs are installed both on the inside- and outside-vacuum chamber walls (see Fig. 4), the accumulated dose is larger on the outside than the inside and becomes smaller with distance from the vacuum chamber. The radiation decreases more rapidly as the distance increases in the vertical direction (Y) compared to the horizontal direction (X). Furthermore, a 1mm-thick lead shield reduces the detected dose to around 1%, indicating that most of the detected radiation is low energy radiation. We therefore believe that most of the radiation comes from scattering of hard synchrotron radiation X-rays from bending magnets.

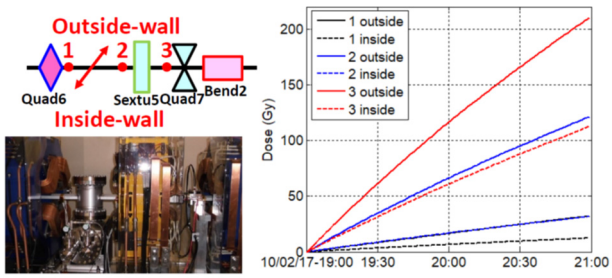


Figure 4: Accumulated radiation dose detected by RadFET at various sites.

## RADIATION STUDY AT POOR VACUUM PRESSURE

During the winter of 2017, the vacuum chamber around the first bending magnet in the 20th cell was replaced in preparation to install a new insertion device requiring a larger vertical photon beam angle aperture. After the replacement, the vacuum pressure near the first bending magnet was around 200 nPa without beam and 6000 nPa with 40 mA stored beam before beam cleaning.

During beam cleaning, a higher counting rate was detected by the PIN-diode BLMs after bending magnets (#3 and 5) of the 20th cell and first bending magnet (#3) in the 21th and 23th cell, as shown in Fig. 5. The high counting rate at the 20th cell is due to inelastic Coulomb scattering of electrons with the residual gas and usually leading to loss in the inside chamber wall downstream from the following bending magnets [6,7]. During top-up at 40 mA, the radiation counting rates of BLM #3, #5 and # 6 in Fig. 6 decrease coming from the improvement of the vacuum pressure as shown in Fig. 7. Note that the decrease of the counting rate for the BLM before the 2nd bending magnet (#4) is limited because most of the radiation comes from bending magnet synchrotron. Therefore, at good vacuum pressure, the count rate in BLM #4 would be larger than elsewhere.

For elastic Coulomb scattering on the residual gas, the electrons are transversally deflected and their betatron oscillation increases [6,7]. The beam can get lost at a location with small aperture and large beta function. For the TPS, the smallest vertical acceptance occurs in the straight sections of the 20th and 22th cell. Therefore, the count rate in BLM #3 is also larger in the 21th cell and 23th cell, shown in the inset of Fig. 5. Similarly, observing the beam current vs. beam loss in the 21th cell in Fig. 8, an obviously high count rate is observed when a beam loss occurs.

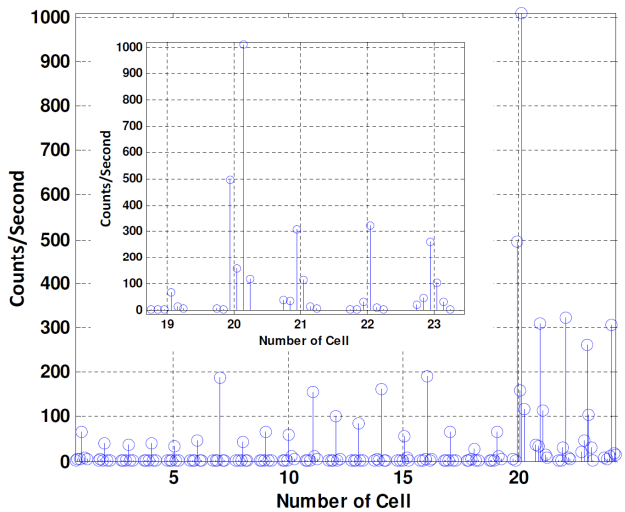


Figure 5: Detected radiation distribution using PIN-diode BLMs for a 40 mA stored beam current after replacing the vacuum chamber in the 20th cell. The inset shows a magnification of the area around the 20th and 21th cells.

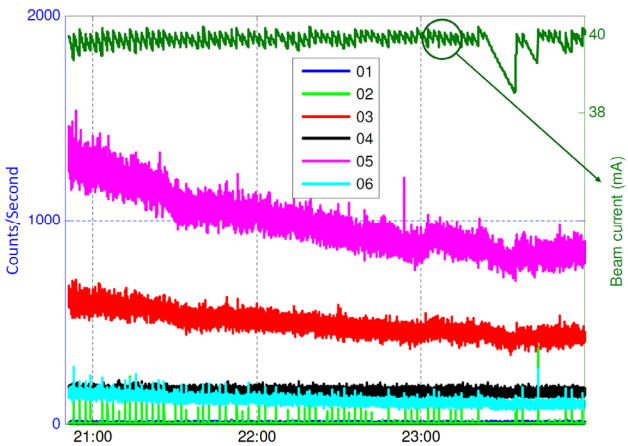


Figure 6: Radiation counting rates during top-up injection at 40 mA for the PIN-diode BLM in the 20th cell.

ISBN: 978-3-95450-184-7 doi:10.18429/JACoW-IPAC2018-WEPAL058

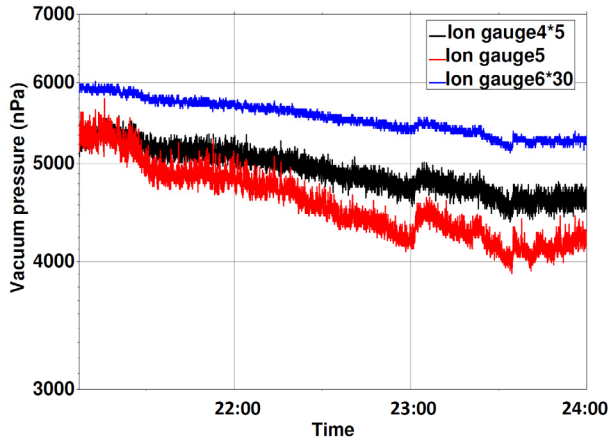


Figure 7: Vacuum pressure in the 20th cell during top-up injection at 40 mA.

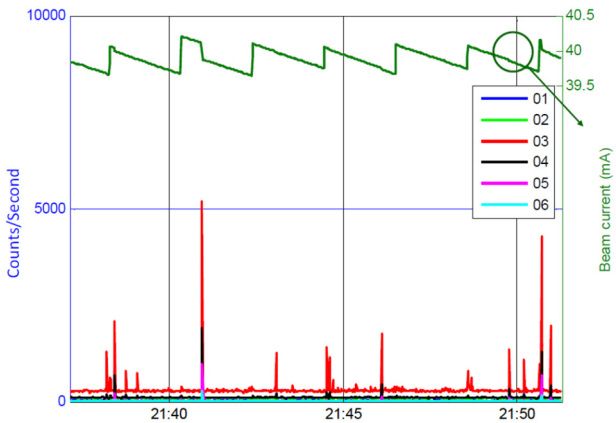


Figure 8: Radiation counting rates during top-up injection at 40 mA for the PIN-diode BLMs in the 21th cell.

## BEAM LOSS STUDIES DURING INJECTION

During top-up injection, we subtract from the radiation counting rates those occurring during decay period to exclude the counting rates coming from synchrotron radiation or from the stored beam during the decay period, as shown in Fig. 9. A high counting rate occurs in several cells. The high counting rate in the 1st cell, 21th and 23th cell come from aperture limitations. This injection loss pattern changes as injection conditions or lattice settings are modified.

As an insertion device gap is changed, the radiation pattern would also change, as shown in Fig. 10. For example, as the gap of the in-vacuum undulator (IU) in the 10th cell is closed to 7 mm, the radiation in the downstream cell (11th cell) becomes much higher, especially after the first bending magnet. The radiation during injection also becomes lager than for the decay period. This effect is not observed when the gap is opened to 40 mm. Furthermore, a residual dose can also be observed downstream from this insertion device. Therefore, the radiation is believed to come from beam losses due to the physical IU aperture as the gap is closed to 7 mm. However, the target of the operation gap in this undulator is 5 mm and the beam lifetime decrease significantly as the gap is smaller than 7 mm. Therefore, the study is still going on to understand the limitation of the gap for operation.

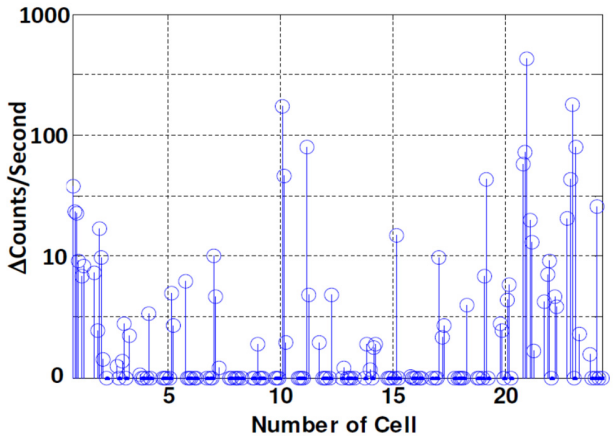


Figure 9: Difference of counting rates during top-up injection and decay.

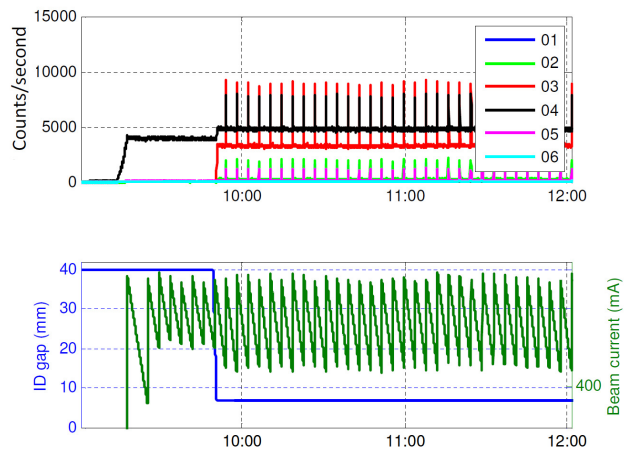


Figure 10: Counting rates of the BLM in the 11th cell as the gap of the in-vacuum undulator changes from 40 mm to 7mm in the 10th cell.

## CONCLUSION

Based on beam loss detector observations, the radiation is highest between the 6th and 7th quadrupole and after the 10th quadrupoles in each cell. That comes from scattering hard synchrotron radiation X-rays generated by bending magnets. During injection, a beam loss can be observed in some cells which could be changed when injection conditions are changed. Beam loss can also be observed downstream from the in-vacuum undulator in the 10th cell as the gap is closed to 7 mm. Minimization of the radiation dose rate can improve injection efficiency.

During vacuum cleaning, elastic Coulomb scattering beam loss occurs at small apertures with large beta function while inelastic Coulomb scattering leads to beam loss beyond downstream bending magnets. The beam loss counts correlate with the vacuum pressure.

ISBN: 978-3-95450-184-7 doi:10.18429/JACoW-IPAC2018-WEPAL058

## REFERENCES


[1] C. C. Kuo *et al.*, "Commissioning of the Taiwan Photon Source", in *Proc. IPAC'15*, Richmond, VA, USA, paper TUXC3, pp. 1314–1318, https://doi.org/10.18429/JACoW-IPAC2015-TUXC3

[2] L. Fröhlich *et al.*, "Online monitoring of absorbed dose in undulator magnets with RADFET dosimeters at FERMI@Elettra", *Nucl. Instr. and Meth. A*, 703 (2013) 77-79.

[3] C. H. Huang *et al.*, "The Beam Loss Monitoring System in the Taiwan Photon Source", in *Proc. IBIC'15*, Melbourne, Australia, Sept. 2015, paper MOPB053, pp. 175–178, https://doi.org/10.18429/JACoW-IBIC2015-MOPB053

[4] D. Lee *et al.*, "Online RadFET Reader for Beam Loss Monitoring System", in *Proc. IPAC'15*, Richmond, VA, USA, paper MOPTY070, pp. 1097–1099, https://doi.org/10.18429/JACoW-IPAC2015-MOPTY070

[5] C. H. Huang *et al.*, "Preliminary Beam Loss Study of TPS during Beam Commissioning", in *Proc. IPAC'16*, Busan, Korea, paper WEPOW039, pp. 2926–2929, https://doi.org/10.18429/JACoW-IPAC2016-WEPOW039

[6] O. A. Konstantinova *et al.*, "Beam Loss Studies for the KEK Compact-ERL", in *Proc. IPAC'14*, Dresden, Germany, June 2017, paper MOPRO109, pp. 349–352, https://doi.org/10.18429/JACoW-IPAC2014-MOPRO109

[7] P. Kuske, "Accelerator Physics Experiments with Beam Loss Monitors at BESSY", in *Proc. DIPAC'01,* Grenoble, France, May 2001, paper IT07, pp. 31-35.